




Luminescence studies of Sm³⁺ doped CdB₄O₇ phosphors

Kamlesh Thakkar¹, Ravi Sharma^{2,*} , Nameeta Brahme¹, D. P. Bisen¹, Anita Verma¹, and Tripti Richhariya³

¹ School of Studies in Physics and Astrophysics, Pt. Ravi Shankar Shukla University, Raipur, C.G., India

² Govt. Arts and Commerce Girls College Devendra Nagar, Raipur, C.G., India

³ Department of Physics, Kalinga University, Naya Raipur, C.G. 492101, India

Received: 29 September 2022

Accepted: 21 April 2023

Published online:

16 May 2023

© The Author(s), under exclusive licence to Springer Science+Business Media, LLC, part of Springer Nature 2023

ABSTRACT

Rare earth Sm³⁺-doped cadmium tetra borate (Cd B₄O₇) phosphors were synthesized by solid-state reaction method. X-ray diffraction (XRD) technique was used for the structural characterization of the prepared phosphors, whereas EDS was used for elemental composition confirmation. The diffraction pattern of the prepared samples is well matched with the standard XRD (JCPDS file no. 30–0204). Photoluminescence emission and excitation spectra for pure and rare earth (Sm³⁺)-doped Cd B₄O₇ phosphor were obtained. The emission spectra of Sm³⁺-doped Cd B₄O₇ showed a characteristic intense emission band at 608 nm along with less intense band at 561 nm and 644 nm under the excitation wavelength of 403 nm. The doping percentage was varied from 1 mol% to 4 mol% of Sm³⁺. The photoluminescence intensity of 2 mol% of Sm³⁺ was found to be highest. From the CIE diagram of the Sm³⁺ doped Cd B₄O₇ phosphor showed the calculated color coordinates in the orange region. The thermoluminescence studies of pure and Sm³⁺-doped samples were carried out. The results of both the samples showed good TL response. The highest TL intensity was observed for 2 mol% of Sm³⁺ concentration. The optimized UV exposure time was 25 min. Nearly 66% linear relation was recorded for total TL intensity and UV exposure time. The TL spectra fall in the orange region, similar to the recorded PL emission spectra.

1 Introduction

Many oxides, sulfides, selenides, tellurides, arsenides, phosphides borates, sulfates, fluorides, and silicates are the important luminescence

materials that have been developed and used over many decades [1]. The optical properties of CdS/ZnS were studied most in earlier times [2]. The borate-based phosphors were studied extensively due to their use in industries and mineralogy. Borate

Address correspondence to E-mail: rvsharma65@gmail.com

materials are interesting because they show excellent mechanical properties, light weight, improved optical properties, and chemical inertness. Their stability under high temperature, low thermal expansion coefficients, and having large electronic band gap make them a potential candidate for research as well as an excellent host lattices for exhibiting luminescence properties [3]. Borate hosts possess variety of structures, low synthetic temperature, transparency to a wide range of wavelengths, and easy preparation methods [4].

Cadmium borate is a metal oxide which is nowadays used to develop new devices. They play a fundamental role due to variety of suitable synthesis techniques. Their physical and chemical properties could be changed with their structures. Cadmium borate possesses various forms and different chemical compositions. The oxygen in borate radical can have both BO_4 and BO_3 (tetrahedral and triangular) forms. Different poly-borate anions groups such as di-borate, tri-borate, and tetra borate can also be formed with these BO_3 and BO_4 groups via common oxygen atoms. Different dopant material can be added to this crystalline material to have different structural properties [5–9].

The impurity element plays a major role to enhance or to change the properties of host materials. Sm^{3+} , Eu^{3+} , Tb^{3+} , and Dy^{3+} are the rare earth activator ions responsible to produce visible light [10–18]. Among the rare earth ions, samarium ($4f^5$) is one of the transition element which has specific advantages. Sm^{3+} -activated luminescent materials have received much attention recently [19–21]. This is due to their ability to exhibit spectral hole burning [22, 23]. The rare earth ions like samarium (Sm^{3+}) can be used as a dopant in diverse crystal hosts for intense emissions in the visible region as it contains large number of closely placed energy levels. Especially, reddish orange emission region from Sm^{3+} -doped materials possesses strong luminescence intensity, large stimulated emission cross section, and high quantum efficiency, which could be suitable for laser applications. So the synthesis of borate phosphor, emitting red luminescence under the UV, or blue light excitation is having great interest for practical applications.

Thermoluminescence (TL) is the phenomenon of light emission from crystalline materials by thermal stimulation, already irradiated by highly ionizing radiations. The irradiation of the sample with suitable ionizing radiation creates electrons and holes trapped over the defect sites present in the material. These trapped electrons jump from trap to conduction band and holes to valance band on heating. With the increase in temperature, the rate of release of electron increases which results in exhibiting radiative or non-radiative emission. For TL dosimetry, the phosphor should have good TL dose sensitivity accuracy and exhibit linearity of dose response over a wide range with nearly no thermal quenching. It must also have the property of reusability. The phosphors are not used as TLDs for all doses but it could be used as TLDs within a specific range of radiation doses, depending on various factors including linearity, precision, dose rate, fading, and reproducibility [24]. The activation energies and frequency factors for different rare earth-doped borate-based samples (TLDs) were reported by the researchers using different methods [24–27].

Our interest to study the luminescence properties of rare earth (Sm^{3+})-doped borates is because of their wide UV transparency, exceptional optical damage thresholds. The excellent chemical, thermal stability and high luminescence have also attracted us and other researchers to study the rare earth-doped borate phosphors [28–35]. The significant practical application of the synthesized borate-based phosphors is the emission of red fluorescence light, when excited under the UV or blue light excitation. The luminescence of borate phosphor and glasses doped with different rare earths has been studied recently [36–40]. In the present work, we have synthesized undoped and Sm^{3+} -doped CdB_4O_7 phosphor with different concentration of Sm^{3+} by solid-state reaction method and studied their photoluminescence properties. The color-correlated temperature is also calculated through CIE coordinate. The X-ray diffraction and EDS are also studied. The thermoluminescence of undoped and Sm^{3+} -doped CdB_4O_7 phosphor, their optimization for UV dose as well as doping concentration, and the TL spectra were also studied.

2 Experimental

In the present work, cadmium tetra borate ($\text{Cd B}_4\text{O}_7$) phosphors were synthesized by solid-state reaction method, at high temperature slightly lower than the melting point of the end product. The raw materials incorporated for the preparation of phosphor were CdCO_3 , H_3BO_3 , and Sm_2O_3 (all of analytical grade). The raw materials were weighed in the appropriate stoichiometric ratio and mixed together by dry grinding, using a mortar and pestle. Once the raw materials were mixed thoroughly, they were transferred to an alumina crucible with a small amount of water and acetone to form slurry (paste). The slurry was then dried on heating around $100\text{ }^\circ\text{C}$ – $200\text{ }^\circ\text{C}$ for one hour. After drying, once again it was ground using a mortar and pestle and sintered in a furnace at $850\text{ }^\circ\text{C}$ temperature in normal atmosphere. After maintaining the sample at this temperature for five hours, the furnace was then switched off. On natural cooling up to $500\text{ }^\circ\text{C}$ temperature, the sample was removed from the furnace and suddenly cooled to room temperature. It is then ground in to fine powder and used for further characterization.

The XRD patterns were obtained over a wide range of Bragg angle 2θ values (10° – 80°) using a Bruker AXS D8 Advance X-ray powder diffractometer (operated at 40 kV) with a $\text{Cu-K}\alpha$ radiation source having wavelength of 1.540598 \AA . Scanning was performed in the 2θ mode with a step size of 0.04 and 1.5 s per step. The scanning electron microscope (SEM) ZEISS EVO 18 available at NIT Raipur was used to capture the SEM images. The powder sample was converted to a normal button size pellet for EDX analysis with the help of Oxford- Energy Dispersive X-ray system (INCA 250 EDS with X-MAX 20 mm) detector. We used UV cabinet that consists of three lamps: a short wavelength UV lamp (254 nm), a long wavelength UV lamp (356 nm), and a visible light lamp facilitated by School of Studies in Physics and Astrophysics, Pt. Ravishankar Shukla University, Raipur, Chhattisgarh, India, for irradiation before the TL recording. A photoluminescence spectrum was recorded using SHIMADZU RF- 5301PC series spectrofluorometer. Thermoluminescence studies were recorded by Nucleonix TL 1009 TLD reader.

3 Result and discussions

The phase characterization of the prepared pure and Sm^{3+} -doped CdB_4O_7 powdered sample was performed by X-ray diffraction. Figure 1 depicts the XRD of pure CdB_4O_7 and different concentration of the Sm^{3+} -doped CdB_4O_7 sample, in which Sm^{3+} varied from $1\text{ mol}\%$ to $4\text{ mol}\%$. The obtained diffraction patterns of pure and Sm^{3+} doped samples were compared with that of reported ones (JCPDS files 30–0204) as well as with each other as shown in Fig. 1. No any extra peak is recorded in the Sm^{3+} -doped samples as compared to the undoped CdB_4O_7 sample. The small amount of doped rare earth ions has virtually no effect on the phase structure. For all the phosphors, the diffraction intensity was found maximum at $(0\ 2\ 1)$ and $(2\ 3\ 0)$ plane having $2\theta = 15.8^\circ$ and 27.7° , respectively, with space group Pbca . The particle size of the samples was found to be 10.4 nm . The particle size was calculated by using Scherer's formula.

Figure 2 shows the crystal structure of cadmium tetra borate in which one cadmium atom is surrounded by six oxygen atom and one boron atom is surrounded by three oxygen atoms. Cadmium tetra borate was crystallized into an orthorhombic structure with $a = 8.704\text{ \AA}$, $b = 14.17\text{ \AA}$, $c = 8.229\text{ \AA}$.

The host lattice contains two cations namely Cd^{2+} and B^{4+} for the occupancy of Sm^{3+} ion. Out of available cations, Sm^{3+} replaces the Cd^{2+} ion. This

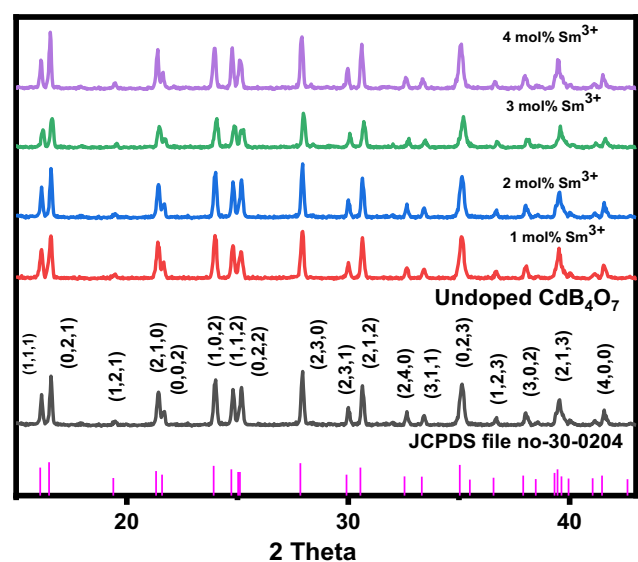


Fig. 1 XRD plot of undoped and CdB_4O_7 : Sm^{3+} ($x = 0.1, 0.2, 0.3, 0.4$) sample

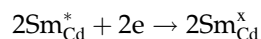
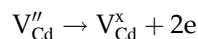
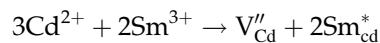
can be confirmed with the help of the formula as shown in Eq. (1), which calculates the radius percentage difference between the doped ion and the substituted cation in the host lattice. The acceptable limit of the radius percentage difference between the cation and the dopant ion must be less than 30% [41]. The calculated radius percentage difference of prepared doped phosphors is listed in Table 1. From the above discussion:

$$D_r = \frac{[R_m(\text{CN}) \sim R_d(\text{CN})]}{R_m(\text{CN})} \times 100\% \quad (1)$$

where D_r is the radius percentage difference between the doped ion and substituted cation, R_m is the ionic radius of the cation, R_d is the ionic radius of the dopant ion, and CN is their coordination number. [42].

The values of D_r between Sm^{3+} and Cd^{2+} on six coordinated sites are 0.84%, while D_r between B^{4+} and Cd^{2+} is 92%. Obviously, the doping ions of Sm^{3+} will clearly substitute the cadmium sites. As trivalent Sm^{3+} ions are doped into CdB_4O_7 , they would non-equivalently replace the Cd^{2+} ions. In order to keep the charge balance, two Sm^{3+} ions would be needed to substitute for three Cd^{2+} ions (the total charge of two trivalent Sm^{3+} ions is equal to that of three Cd^{2+} ions). Hence, one vacancy defect of V_{Cd}'' with two negative charges and two positive defects of Sm_{Cd}^x would be created by each substitution of every two Sm^{3+} ions in the compound. The vacancy V_{Cd}'' would

act as a donor of electrons, while the two Sm_{Cd}^x defects become acceptors of the electrons. Consequently, by thermal stimulation, the negative charges in the vacancy defects of V_{Cd}'' would be transferred to the Sm^{3+} sites and reduce Sm^{3+} to Sm^{2+} . The whole process can be expressed by the following equations:



3.1 SEM and EDX analysis

The SEM images were obtained to study the morphology and microstructure of the prepared sample as shown in the Fig. 3. SEM image of the microcrystalline powder samples with some agglomeration among the crystalline grain and an irregular morphology can be seen clearly for undoped CdB_4O_7 sample. The irregular flower type, micro-size crystallite structures for Sm-doped sample could also be seen in the SEM images.

EDX measurements were performed to determine the composition of the prepared CdB_4O_7 and $\text{CdB}_4\text{O}_7:\text{Sm}^{3+}$ samples (Fig. 4). The selected area diffraction pattern was also performed for characterizing the compositions of the borate microcrystalline powder. The EDX spectrum confirms the elemental composition and the stoichiometric ratio of the materials used in synthesizing the CdB_4O_7 and $\text{CdB}_4\text{O}_7:\text{Sm}^{3+}$ samples. The spectrum also confirms the doping of rare earth element (Sm^{3+}) in the CdB_4O_7 sample.

3.2 Photoluminescence studies

The photoluminescence properties of pure and Sm^{3+} -doped CdB_4O_7 host were investigated by the excitation and emission spectra at room temperature. The excitation spectra of pure CdB_4O_7 in the range of 200–550 nm are shown in Fig. 5a with fixed emission wavelength of 608 nm, whereas Fig. 5b shows the emission spectra of pure CdB_4O_7 excited at 405 nm. The excitation spectra show four peaks at 244 nm, 328 nm, 346 nm, and 405 nm, respectively. The

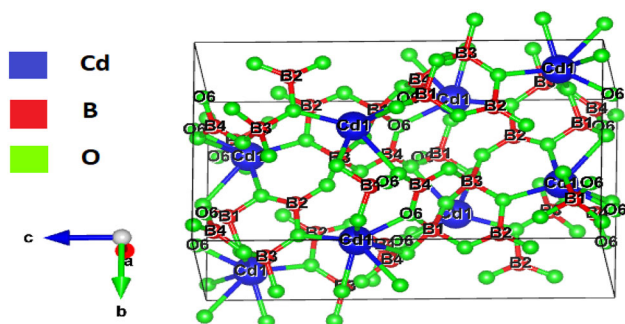


Fig. 2 Crystal structure of CdB_4O_7

Table 1 Radius percentage difference between dopant and cation of the host

S.N	Cation $R_m(\text{CN})$	Dopant $R_d(\text{CN})$	
	Cd^{2+}	B^{4+}	Sm^{3+}
Ionic radius (CN)	0.95(6)	0.11(4)	0.958(6)
D_r (radius percentage difference)	0.84%	92%	

Fig. 3 SEM images of undoped CdB_4O_7 and $\text{CdB}_4\text{O}_7: 2 \text{ mol}\% \text{ Sm}^{3+}$ sample

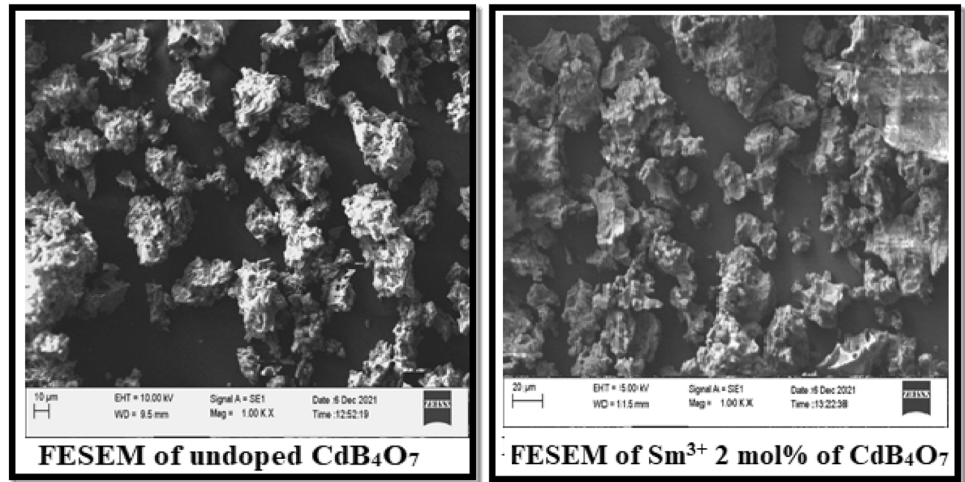


Fig. 4 EDX pattern of undoped CdB_4O_7 and $\text{CdB}_4\text{O}_7: 2 \text{ mol}\% \text{ Sm}^{3+}$ phosphor

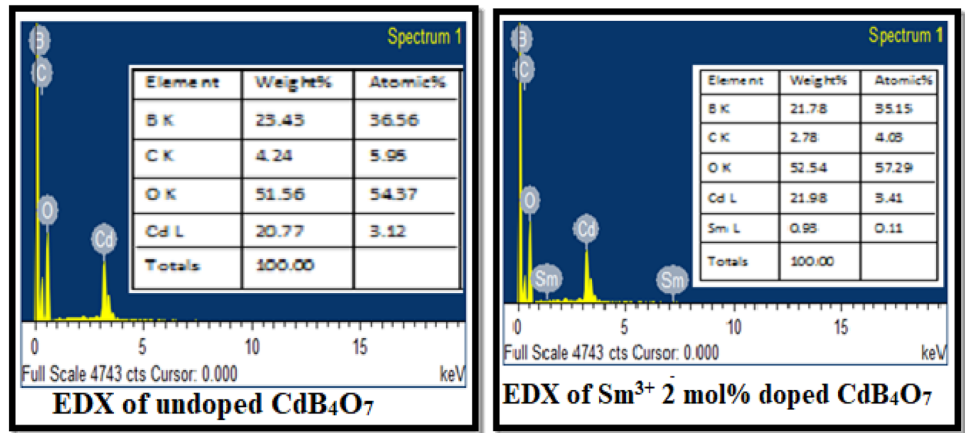
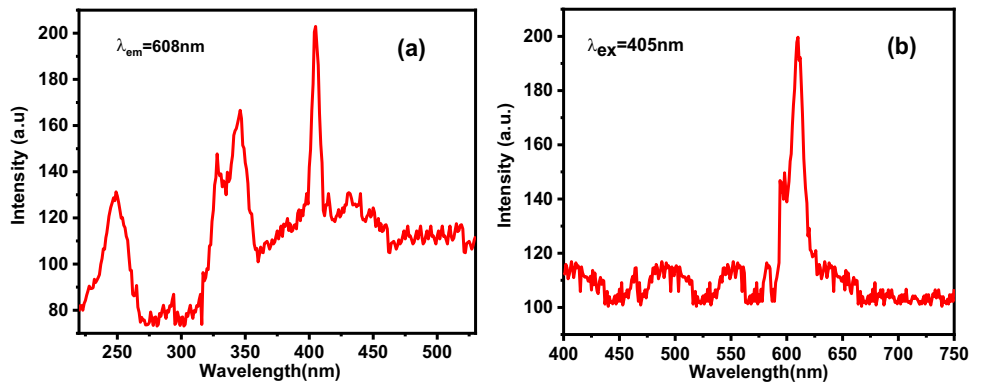


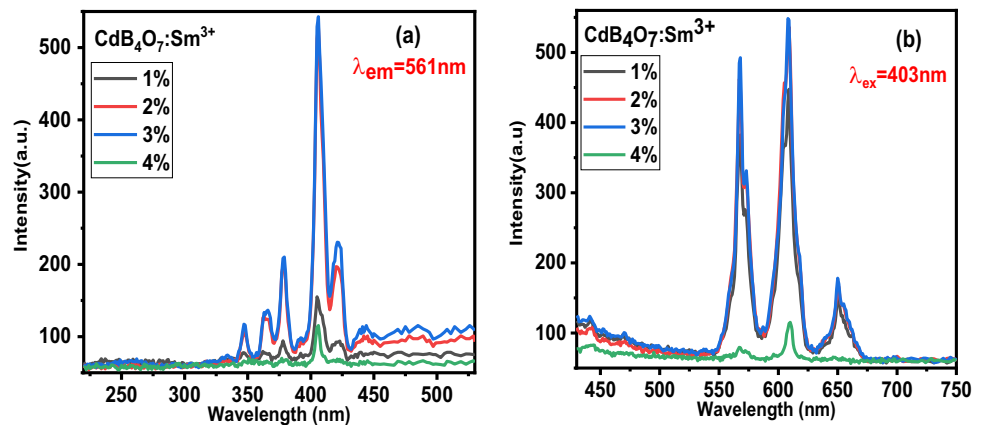
Fig. 5 Photoluminescence excitation and emission spectra of pure CdB_4O_7 sample



highest intensity peak was obtained at 405 nm. So, for recording emission spectra, all the samples were excited at 405 nm. The emission peak was recorded at 608 nm in the orange color region.

Figure 6 shows the photoluminescence excitation spectra (Fig. 6a) and emission spectra (Fig. 6b) of Sm^{3+} -doped CdB_4O_7 phosphor. The doping percentage of Sm^{3+} was changed from 1 mol % to

Fig. 6 Photoluminescence excitation and emission spectra of $\text{CdB}_4\text{O}_7:\text{Sm}^{3+}$ phosphor



4 mol% for recording excitation spectra and the emission spectra. The excitation spectra showed five peaks at 347 nm, 364 nm, 376 nm, 403 nm, and 419 nm corresponding to the transitions from ${}^6\text{H}_{5/2}$ to, ${}^4\text{D}_{3/2}$, ${}^4\text{P}_{7/2}$, ${}^4\text{P}_{3/2}$, ${}^4\text{P}_{5/2}$, and ${}^4\text{G}_{9/2}$, levels respectively [43, 44]. The dominant peak was found at 403 nm, hence chosen as the excitation wavelength (λ_{ex}) for the determination of the emission spectra. The emission wavelength was fixed at 561 nm. The excitation peak intensities were found changing with the varying concentrations of Sm^{3+} , whereas the peak positions remain unchanged. This is due to their intra-configurational (f–f) transitions. The other less intense peaks suggest that by changing the excitation wavelength, the emission intensity could be tailored.

The emission spectra of $\text{CdB}_4\text{O}_7:\text{Sm}^{3+}$ phosphor are reported under the fixed excitation wavelength at 403 nm (Fig. 6b). The emission spectra showed three peaks, first two at yellow (561 nm) and orange (608 nm) region and the third peak was found at orange – red region (644 nm). These peaks are corresponding to ${}^4\text{G}_{5/2} \rightarrow {}^6\text{H}_{5/2}$, ${}^4\text{G}_{5/2} \rightarrow {}^6\text{H}_{7/2}$, and ${}^4\text{G}_{5/2} \rightarrow {}^6\text{H}_{9/2}$, respectively. Among the peaks, the peak located at 608 nm, i.e., ${}^4\text{G}_{5/2} \rightarrow {}^6\text{H}_{7/2}$ transition, has the highest intensity. This is due to both electric and magnetic dipole transition. The PL intensity was found to be increasing for increasing percentage of Sm^{3+} and becomes maximum for 2 mol% of Sm^{3+} . For higher concentration, the PL intensity starts decreasing due to concentration quenching effect. The peak at ${}^4\text{G}_{5/2} \rightarrow {}^6\text{H}_{9/2}$ due to electric dipole transition is less intense than the peak at ${}^4\text{G}_{5/2} \rightarrow {}^6\text{H}_{5/2}$ due to magnetic dipole transition [44, 45].

4 CIE diagram

CIE 1931 is a color-matching system by which numerically specified color could be measured. Color coordinate is used to determine the color of phosphor. The coordinates are plotted in 3D chromaticity. CIE of chromaticity coordinate for Sm^{3+} -doped CdB_4O_7 is shown in Fig. 7. Correlated color temperature is calculated by using X–Y coordinate system from CIE 1931 as shown in the Table 2. The lower value of color purity indicates the purity of white light emission [46]. It is clear from the above analysis that the $\text{CdB}_4\text{O}_7:\text{Sm}^{3+}$ phosphor is not a cool white light application for outdoor illumination.

$$\text{CCT} = -449 n^3 + 3525 n^2 - 6823 n + 5520.33$$

where $n = (x - x_e)/(y - y_e)$ and $x_e = 0.5532$ and $y_e = 0.4459$

The CCT calculated is 1981 K; hence, prepared phosphor shows warm appearance.

4.1 Thermoluminescence studies

Thermoluminescence (TL) is defined as the emission of light from a semiconductor or an insulator when it is heated, due to the previous absorption of energy from irradiation. All types of radiation such as α rays, β rays, γ rays, and UV rays can excite a material, but to widely different extent. We have used UV radiation as it is available in the department. Due to irradiation, electrons and holes are created. On heating, they are released from the traps and recombine to give thermoluminescence. Thermoluminescence properties of undoped CdB_4O_7 phosphor and the

Fig. 7 CIE Chromaticity Coordinate Diagram 1931 of CdB₄O₇: Sm³⁺ Sample

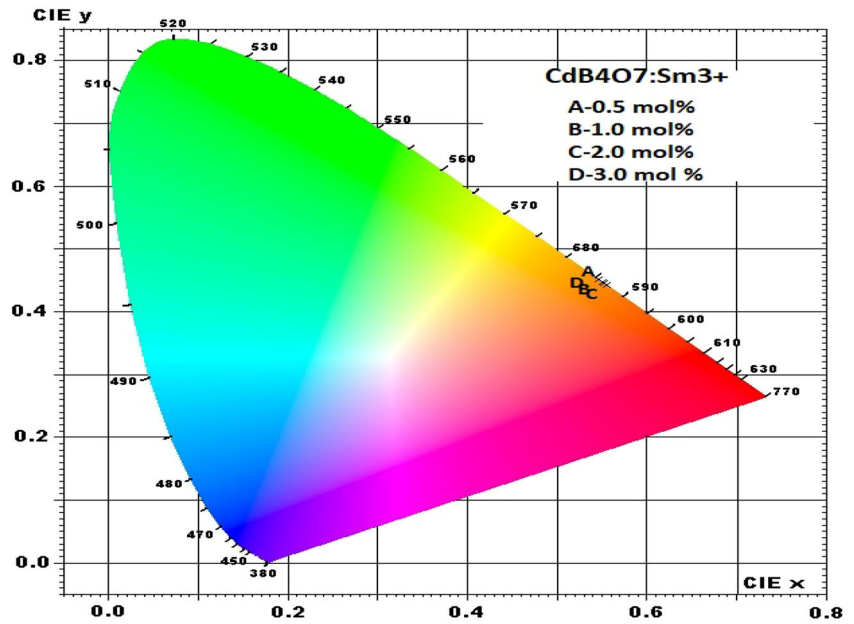


Table 2 CIE chromaticity coordinate, color purity, and CCT

Sample	CIE chromaticity coordinate		Color purity	Correlated color temperature (K)
	x	y		
CdB ₄ O ₇ :(0.005) Sm ³⁺	0.5478	0.4512	86.24 × 10 ⁻²	2062
CdB ₄ O ₇ :(0.01) Sm ³⁺	0.5532	0.4459	86.51 × 10 ⁻²	1981
CdB ₄ O ₇ :(0.02) Sm ³⁺	0.5572	0.4419	87.06 × 10 ⁻²	1942
CdB ₄ O ₇ :(0.03) Sm ³⁺	0.5526	0.4465	86.36 × 10 ⁻²	2001

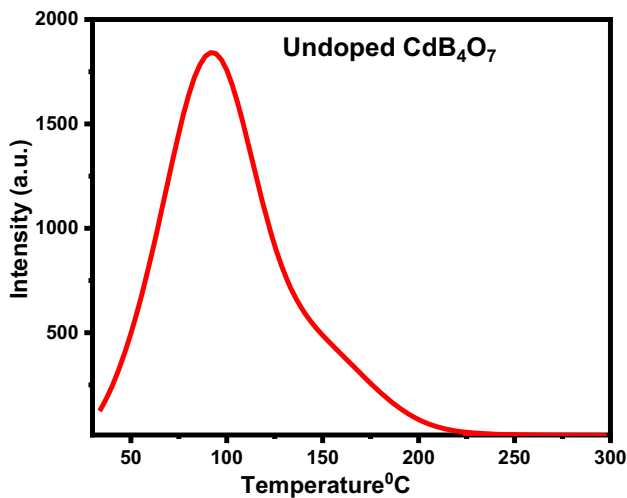


Fig. 8 TL glow curve of undoped CdB₄O₇ phosphor

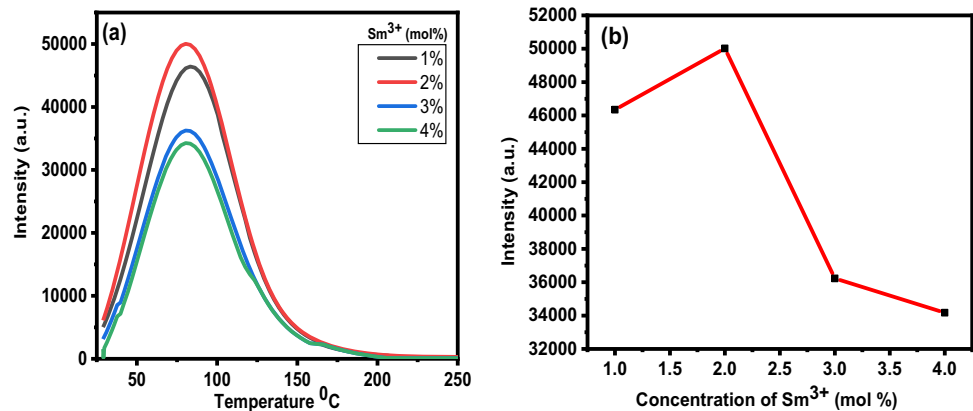
effect of doping are investigated. TL glow curves of the phosphors were optimized for doping concentration and also with varying UV exposure time. The

heating rate was fixed at 5°C/s for all measurements. All the samples were heated up to 300°C from room temperature.

Figure 8 shows the TL glow curve of undoped CdB₄O₇ phosphor. The sample was irradiated for 15 min UV exposure time. A single peak was observed with peak centered at 96 °C with a small shoulder-like structure at 157 °C.

TL glow curve of Sm³⁺-doped CdB₄O₇ is shown in Fig. 9a. We observed a single peak in the TL glow curve centered at 83 °C. The TL intensity of samples increased with increasing doping concentration and achieved the highest value. On further increase in the Sm³⁺ concentration, the TL intensity decreases; this is due to concentration quenching effect [47]. The TL intensity varies with concentration but the shape of the peak does not change with concentration. Normally, TL peak position is independent of the dopant element and exhibits no shift with change in doping but in our case, a small shift in the peak is observed.

Fig. 9 TL glow curve of CdB₄O₇:xSm³⁺ phosphor and TL Vs Sm³⁺ concentration



This may be due to the characteristic of dopant that has caused the creation of traps at different levels in the bandgap of the material. It may also be due to the mismatch of size of the RE ions incorporated in the host crystal introducing lattice strains.

When Sm³⁺ doping concentration exceeds a particular limit, the distance between the Sm³⁺ luminescent centers decreases which results in non-radiative energy transfer. The critical distance (R_c) between the activated ions in phosphors can be evaluated by the below formula given by the Eq. (2)[48]

$$R_c \approx 2 \left[\frac{3V}{4\pi x_c N} \right]^{1/3} \quad (2)$$

where N is the host cations in per unit cell, x_c represents the critical concentration of Sm³⁺, and V is the volume of the unit cell. By taking the appropriate values of N , V , and x_c , R_c is estimated to be 11 Å, which was greater than 5 Å, indicating that the concentration quenching mechanism of Sm³⁺ ions was mainly ascribed to the multipole–multipole interaction.

Figure 9b shows TL intensity of CdB₄O₇:xSm³⁺ phosphor with different doping concentration of Sm³⁺ ($x = 0.1, 0.2, 0.3, 0.4$). The maximum TL intensity was achieved for 2 mol% of Sm³⁺ and then the decrease in TL intensity was observed with increasing doping concentration. As we increase the impurity concentration, there is an increase in the number of defects/traps which in turn implies a growth in the density of charge carriers being trapped upon irradiation. Therefore, the initial rise in the TL peak intensity occurred. Furthermore, on being thermally stimulated, these charge carriers release from traps which in turn recombine with their counterparts at

the recombination center and exhibit TL glow peaks [49].

Figure 10a shows the TL glow curve of undoped CdB₄O₇ phosphor with varying UV exposure time.. It is seen from the figure that the thermoluminescence signals increases with increasing UV exposure time and the thermoluminescence signals becomes maximum for 15 min of UV exposure and then starts decreasing. This is due to the charge carrier density that has been increased with increasing UV exposure time. More the radiation dose, more will be the creation of numbers of electron–holes, which causes increase in the TL intensity. After a particular UV dose, the TL intensity seems to be saturated, as no more traps are available for further irradiation. After 15 min of UV exposure time, destruction in trap level resulted in the decrease of thermoluminescence signals. Figure 10b exhibits the effect of UV exposure time on the TL intensity for undoped CdB₄O₇ phosphor.

Figure 11a, b shows the effect of UV exposure time on the TL glow curve of Sm³⁺ doped CdB₄O₇ phosphor. It is clear that initially the TL intensity increases with increase in exposure time and attains the highest value at 25 min of UV dose and the TL intensity then decreases with increasing exposure time. Similar shape of the glow curve was recorded for different exposure times.

The variation in the TL intensity with the UV exposure time is shown in Fig. 12a for undoped CdB₄O₇ and 12b for Sm³⁺-doped CdB₄O₇ phosphor. In the inset Fig. 12a, b, it was found that the TL intensity first reached a maximum and then either declined (see Fig. 12b) or after a sharp fall, further very less declination is achieved (see Fig. 12a). Since thermoluminescence dosimeters should have a wide

Fig. 10 a TL glow curve of undoped CdB_4O_7 phosphor with varying UV exposure time. b TL intensity Vs different UV exposure time

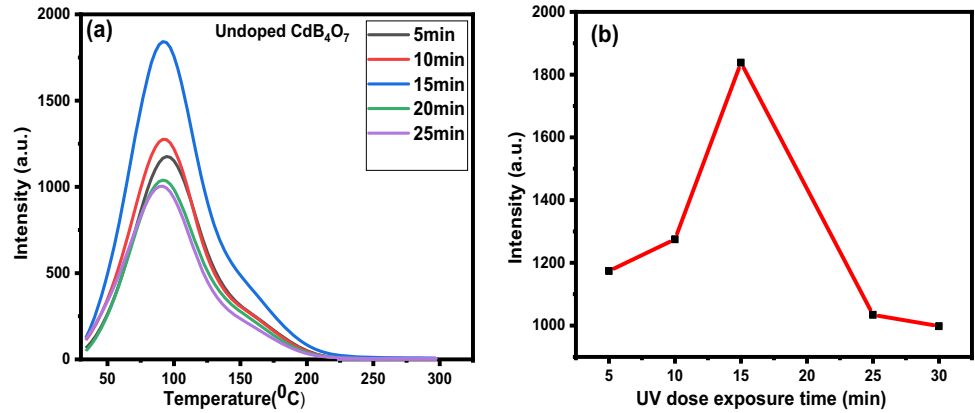


Fig. 11 a TL glow curve of Sm^{3+} doped CdB_4O_7 phosphor with different UV dose. b TL intensity Vs UV exposure time

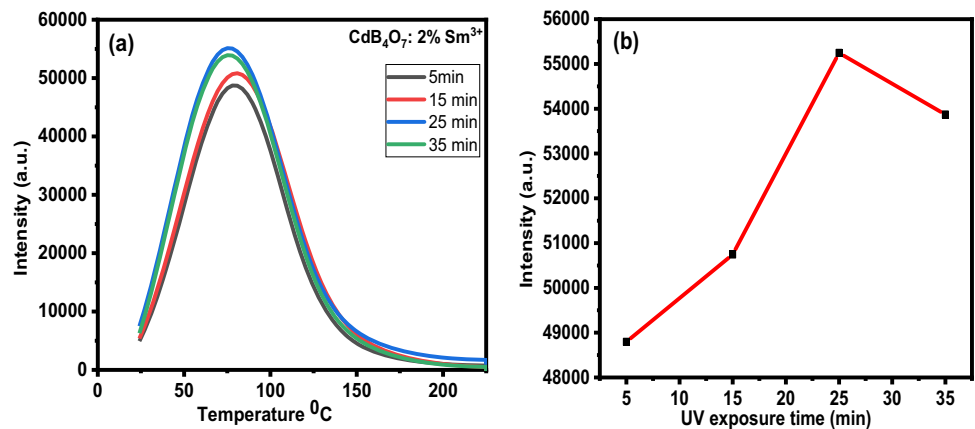
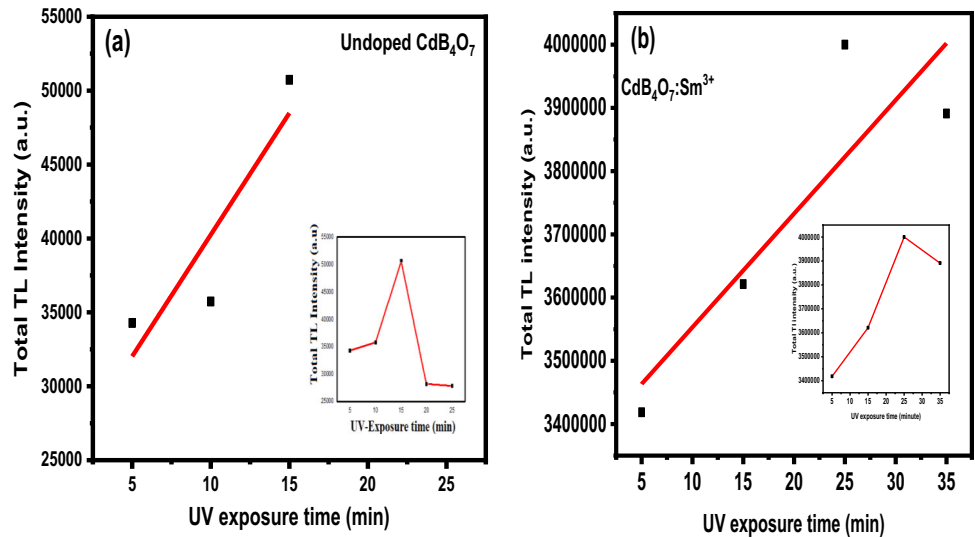


Fig. 12 Total TL intensity Vs UV exposure time for undoped and Sm^{3+} -doped phosphor



interval in which the luminescence intensity is linear with the absorbed dose, the data corresponding to total TL intensity versus UV exposure time were fitted (Fig. 12). We have used origin software to plot the

data of UV exposure time versus total TL intensity and the equation for linear fit $y = a + bx$ for tracing those points. If the value of Adj R- Square is 0.99, it means the data are almost linear. Our data showed

Fig. 13 Deconvoluted TL peaks for **a** of CdB_4O_7 and **b** $\text{CdB}_4\text{O}_7:\text{Sm}^{3+}$ phosphors

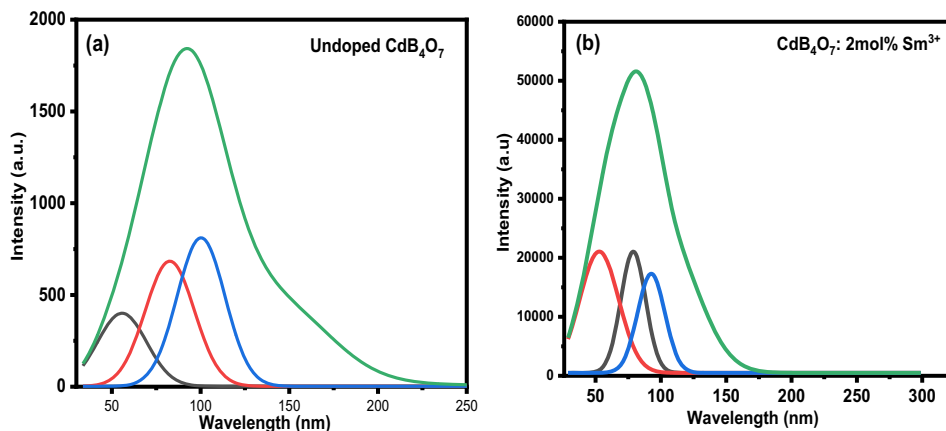
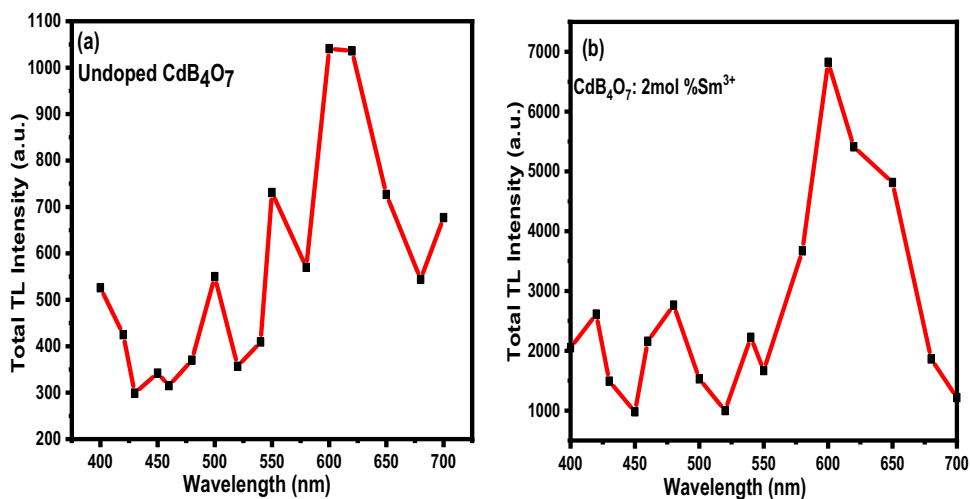


Table 3 The trapping parameters of undoped and Sm^{3+} -doped phosphors

Phosphor	Peak	T_m (K)	τ (K)	δ (K)	ω	μ_g	E(eV)	$S(\text{s}^{-1})$
Undoped CdB_4O_7	1	328.8	16.2	16.4	32.6	0.5	0.9	1.60×10^{15}
	2	355.7	16.6	16.7	33.3	0.5	1	1.01×10^{16}
	3	373.3	15.7	16.1	31.8	0.5	1.2	6.07×10^{17}
$\text{CdB}_4\text{O}_7:\text{Sm}^{3+}$	1	325.9	18.6	17.79	36.39	0.488	0.75	8.9×10^{12}
	2	351.91	11.71	11.26	22.97	0.49	1.43	1.3×10^{22}
	3	365.32	12.12	13.049	25.16	0.51	1.54	6.9×10^{22}

Fig. 14 TL emission spectra of undoped CdB_4O_7 and $\text{CdB}_4\text{O}_7:\text{Sm}^{3+}$ phosphor



the value of Adj R-Square to be 0.66528. It means the data are approximately 66% linear, i.e., not perfectly linear.

Gaussian curve fitting peaks are represented in Fig. 13a and b. Broad peaks of pure and Sm^{3+} -doped CdB_4O_7 contain three peaks in Fig. 13a and three peaks in Fig. 13b, respectively. Each TL peak is associated with certain trap levels that lie within the forbidden gap. The traps are characterized by intrinsic kinetic parameters which may be retrieved

from TL data [50–53]. In glow curve analysis, the kinetic parameters such as activation energy (E), frequency factor (S), geometrical shape factor $\mu_g = \delta/\omega$, where $\delta = T_2 - T_M$, $\omega = T_2 - T_1$, $\tau = \tau_1$, and order of kinetics (b) were calculated through Chen's peak shape method after using the deconvolution of the peak. The peaks are numbered according to the computerized glow curve deconvolution (CGCD) technique to analyze the TL glow curves. The program automatically finds and can fit ten overlapping

glow peaks at a time. In our case, it showed three peaks. The calculated trapping parameters of phosphors are shown in the Table 3. An increase in the activation energy with rise in temperature was recorded which indicates the existence of deeper trap at the temperature where maximum TL intensity is obtained (T_m) and shallower traps at lower temperature. Apart from the temperature T_m , some other factors also influence activation energy such as frequency factor (S), order of kinetics (b), etc. In our case, the calculated order of kinetics was $b = 2$.

TL emission spectra are the graph between total TL intensity versus the wavelength. Figure 14a, b are the TL spectra of undoped CdB_4O_7 and $\text{CdB}_4\text{O}_7:\text{Sm}^{3+}$ (2 mol%) phosphor, respectively. These spectra were recorded through band pass filter in the range of 400 to 700 nm. From the figure, it is clearly seen that one major peak centered at 608 nm is obtained, which corresponds to ${}^4\text{G}_{5/2} \rightarrow {}^6\text{H}_{7/2}$ transition of Sm^{3+} ion for both undoped and Sm^{3+} -doped CdB_4O_7 phosphor. This suggests that TL emission spectra show resemblance with PL spectra.

5 Conclusions

Pure CdB_4O_7 and $\text{CdB}_4\text{O}_7:\text{Sm}^{3+}$ phosphors were successfully synthesized by solid-state reaction method. The XRD analysis confirms the orthorhombic phase structure of the synthesized phosphor. EDX measurements of the prepared CdB_4O_7 and $\text{CdB}_4\text{O}_7:\text{Sm}^{3+}$ samples confirm the elemental composition and stoichiometric ratio. It also confirms the incorporation of Sm^{3+} ion in the sample. The excitation spectra of the Sm^{3+} -doped sample, showed five peaks at 347 nm, 364 nm, 376 nm, 403 nm, and 419 nm, corresponding to the transitions from ${}^6\text{H}_{5/2}$ to, ${}^4\text{D}_{3/2}$, ${}^4\text{P}_{7/2}$, ${}^4\text{P}_{3/2}$, ${}^4\text{P}_{5/2}$, and ${}^4\text{G}_{9/2}$. The emission spectra showed three peaks at 561 nm (yellow), 608 nm (orange), and at 644 nm (orange – red region) corresponding to ${}^4\text{G}_{5/2} \rightarrow {}^6\text{H}_{5/2}$, ${}^4\text{G}_{5/2} \rightarrow {}^6\text{H}_{7/2}$, and ${}^4\text{G}_{5/2} \rightarrow {}^6\text{H}_{9/2}$ transitions, respectively. The peak at 600 nm, i.e., ${}^4\text{G}_{5/2} \rightarrow {}^6\text{H}_{7/2}$ transition, showed highest intensity. For the sample with 2% of Sm^{3+} , the PL intensity was found to be maximum. Further increase in the concentration of Sm^{3+} showed concentration quenching effect. The efficient energy transfer to the luminescence center from the host matrix was also recorded. The CIE coordinate was found at $X = 0.5867$ and $Y = 0.4126$. This indicates that the

prepared phosphor is a potential candidate for the orange light-emitting diodes. It could also be used for the solid-state laser applications. The optimized doping (Sm^{3+}) concentration for thermoluminescence of CdB_4O_7 phosphor was 2 mol% and the optimized UV dose for the Sm^{3+} -doped CdB_4O_7 sample was 25 min. TL and PL spectra of the samples were recorded in the same orange region, which indicates that they are originated from same luminescence center.

Author contributions

All authors contributed to the study conception and design. Material preparation, data collection, and analysis were performed by KT, RS, NB, DPB, and TR. The first draft of the manuscript was written by RS and all authors commented on previous versions of the manuscript. All authors read and approved the final manuscript.

Funding

The authors declare that no funds, grants, or other support was received during the preparation of this manuscript.

Data availability

The datasets generated during and/or analyzed during the current study are available from the corresponding author on reasonable request.

Declarations

Competing interests The authors have no relevant financial or non-financial interests to disclose.

References

1. C.J. Peacock, J. Chem. Technol. Biotechnol. **46**, 252 (2007)
2. D. Patidar, K.S. Rathore, N.S. Saxena, K. Sharma, T.P. Sharma, J. Nano Res. **3**, 97 (2008)
3. V.P. Hedao, V.B. Bhatkar, S.K. Omanwar, Int. Ref. J. Eng. Sci. **1**, 34 (2012)

4. A. Lavat, C. Graselli, M. Santiago, J. Pomarico, E. Caselli, *Cryst. Res. Technol.* **39**, 840 (2004)
5. C. A. Giúdice and J. C. Benítez, *Prog Org Coat* **42**, 82 (2001).
6. D.-G. Chen, W.-D. Cheng, D.-S. Wu, H. Zhang, Y.-C. Zhang, Y.-J. Gong, Z.-G. Kan, *Solid State Sci.* **7**, 179 (2005)
7. A. Ivankov, J. Seekamp, W. Bauhofer, *Mater. Lett.* **49**, 209 (2001)
8. D.M. Schubert, M.Z.V. Fazlul Alam, C.B. Knobler, *Chem. Mater.* **15**, 866 (2003)
9. L.K. Limbach, P. Wick, P. Manser, R.N. Grass, A. Bruinink, W.J. Stark, *Environ Sci Technol* **41**, 4158 (2007)
10. R. Cao, Z. Jiang, T. Chen, H. Liang, X. Yi, Y. Zhong, H. Zhang, W. Luo, *J Lumin* **243**, 118618 (2022)
11. N. Sooraj Hussain, G. Hungerford, R. El-Mallawany, M. J. M. Gomes, M. A. Lopes, Nasar Ali, J. D. Santos, and S. Budhudu, *J. Nanosci. Nanotechnol.* **9**, 3672 (2009).
12. M. Que, Z. Ci, Y. Wang, G. Zhu, Y. Shi, S. Xin, *J. Lumin.* **144**, 64 (2013)
13. A. Tang, D.-F. Zhang, L. Yang, *J. Lumin.* **132**, 1489 (2012)
14. S.A. Naidu, S. Boudin, U.V. Varadaraju, B. Raveau, *J. Electrochem. Soc.* **159**, J122 (2012)
15. X. Dong, J. Zhang, X. Zhang, Z. Hao, S. Lv, *Ceram. Int.* **40**, 5421 (2014)
16. P. Abdul Azeem, M. Kalidasan, R.R. Reddy, K. Ramagopal, *Opt. Commun.* **285**, 3787 (2012)
17. E. Cavalli, P. Boutinaud, R. Mahiou, M. Bettinelli, P. Dorenbos, *Inorg. Chem.* **49**, 4916 (2010)
18. A. Boukhris, M. Hidouri, B. Glorieux, M. Ben Amara, *Mater. Chem. Phys.* **137**, 26 (2012)
19. R. Cao, W. Wang, Y. Ren, Z. Hu, X. Zhou, Y. Xu, Z. Luo, A. Liang, *J. Lumin.* **235**, 118054 (2021)
20. Y. Zhang, C. Lu, L. Sun, Z. Xu, Y. Ni, *Mater. Res. Bull.* **44**, 179 (2009)
21. M. Sobczyk, P. Starynowicz, R. Lisiecki, W. Ryba-Romanowski, *Opt Mater (Amst)* **30**, 1571 (2008)
22. J. Zhu, K. Zhu, L. Chen, *J Non Cryst Solids* **352**, 150 (2006)
23. K. Machida, G. Adachi, J. Shiohara, *J Lumin* **21**, 101 (1979)
24. T. A. Joseph, V. Chopra, M. Michalska-Domanska, and S. J. Dhoble, *Radiation Dosimetry Phosphors* **45** (2022).
25. H. Komiya, I. Kawamura, H. Kawamoto, Y. Fujimoto, M. Koshimizu, G. Okada, Y. Koba, G. Wakabayashi, K. Asai, *Jpn J Appl Phys* **61**, 1007 (2022)
26. V. Chopra, Y. R. Parauha, D. Poelman, and S. J. Dhoble, in *Radiation Dosimetry Phosphors* (Elsevier, 2022), pp. 27–45.
27. V. Dubey, N. Dubey, J. Kaur, J. Singh, T. Ramarao, M. Pandey, and S. J. Dhoble, in *Radiation Dosimetry Phosphors* (Elsevier, 2022), pp. 299–327.
28. R. Stefani, A.D. Maia, E.E.S. Teotonio, M.A.F. Monteiro, M.C.F.C. Felinto, H.F. Brito, *J Solid State Chem* **179**, 1086 (2006)
29. Y.-H. Won, H. S. Jang, W. bin Im, and D. Y. Jeon, *J Electrochem Soc* **155**, J226 (2008).
30. M. Ayvacikli, A. Ege, N. Can, *Opt. Mater. (Amst)* **34**, 138 (2011)
31. Y. Yang, Z. Ren, Y. Tao, Y. Cui, H. Yang, *Curr. Appl. Phys.* **9**, 618 (2009)
32. D. Tu, Y. Liang, R. Liu, Z. Cheng, F. Yang, W. Yang, *J. Alloys Compd.* **509**, 5596 (2011)
33. J. Hao, J. Gao, M. Cocivera, *Appl. Phys. Lett.* **82**, 2778 (2003)
34. A.E. Henkes, R.E. Schaak, *J. Solid State Chem.* **181**, 3264 (2008)
35. G. Ju, Y. Hu, H. Wu, Z. Yang, C. Fu, Z. Mu, F. Kang, *Opt Mater (Amst)* **33**, 1297 (2011)
36. A. Bajaj, A. Khanna, B. Chen, J.G. Longstaffe, U.-W. Zwanziger, J.W. Zwanziger, Y. Gómez, F. González, *J Non Cryst Solids* **355**, 45 (2009)
37. A. Oza, V. Ojha, S. Dhale, S. Dhoble, *Luminescence* **37**, 1563 (2022)
38. M. Sonsuz, M. Topaksu, J. Hakami, N. Can, *Radiat. Phys. Chem.* **201**, 110412 (2022)
39. X. Zhu, C. Mai, M. Li, *J Non Cryst Solids* **388**, 55 (2014)
40. M Parandamaiah, S Venkatramana Reddy, and K Naveen Kumar, *Inter. J. Engi. Science Invention Re. & Development* **2**, (2016).
41. B. Verma, R.N. Baghel, D.P. Bisen, N. Brahme, A. Khare, *J. Alloys Compd.* **805**, 663 (2019)
42. S. Kasturi, V. Sivakumar, U.V. Varadaraju, *Luminescence* **32**, 334 (2017)
43. V.B. Sreedhar, Ch. Basavapoomima, C.K. Jayasankar, *J. Rare Earths* **32**, 918 (2014)
44. L.F. Shen, B.J. Chen, E.Y.B. Pun, H. Lin, *J Lumin* **160**, 138 (2015)
45. S. Shanmuga Sundari, K. Marimuthu, M. Sivraman, and S. S. Babu, *J Lumin* **130**, 1313 (2010).
46. K.V. Krishnaiah, K.U. Kumar, C.K. Jayasankar, *Mater. Express* **3**, 61 (2013)
47. R. Chen, J.L. Lawless, V. Pagonis, *Radiat. Meas.* **46**, 1380 (2011)
48. G. Blasse, B.C. Grabmaier, *Luminescent Materials* (Springer, Berlin Heidelberg, Berlin, Heidelberg, 1994)
49. K. Sharma, S. Bahl, B. Singh, P. Kumar, S.P. Lochab, A. Pandey, *Radiat. Phys. Chem.* **145**, 64 (2018)
50. D.J. Daniel, O. Annalakshmi, U. Madhusoodanan, P. Ramasamy, *J. Rare Earths* **32**, 496 (2014)
51. N. Kaur, M. Singh, L. Singh, S.P. Lochab, *Radiat. Phys. Chem.* **87**, 26 (2013)
52. A. Kadari, S. Delice, N.M. Gasanly, *Optik (Stuttg)* **138**, 372 (2017)

53. M. Mashangva, N. Singh, & Th, and B. Singh, *Estimation of Optimal Trapping Parameters Relevant to Persistent Luminescence* (2011).

Publisher's Note Springer Nature remains neutral with regard to jurisdictional claims in published maps and institutional affiliations.

Springer Nature or its licensor (e.g. a society or other partner) holds exclusive rights to this article under a publishing agreement with the author(s) or other rightsholder(s); author self-archiving of the accepted manuscript version of this article is solely governed by the terms of such publishing agreement and applicable law.